J. Fluid Mech. (2001), *vol.* 437, *pp.* 29–43. Printed in the United Kingdom

Mass flow and tangential momentum accommodation in silicon micromachined channels

By ERROL B. ARKILIC[1], KENNETH S. BREUER[2] AND MARTIN A. SCHMIDT[3]

[1]Phasyn, San Carlos, CA 94070, USA

[2]Division of Engineering, Brown University, Providence RI 02912, USA

[3]Microsystems Technology Laboratories, Massachusetts Institute of Technology, Cambridge, MA 02139, USA

(Received 4 October 1999 and in revised form 18 December 2000)

High-precision experimental results are reported showing the tangential momentum accommodation coefficient (TMAC) for several gases in contact with single-crystal silicon to be less than unity. A precise and robust experimental platform is demonstrated for measurement of mass flows through silicon micromachined channels due to an imposed pressure gradient. Analytic expressions for isothermal Maxwellian slip flows through long channels are used to determine the TMAC at a variety of Knudsen numbers. Results from experiments using nitrogen, argon and carbon dioxide are presented. For all three gases the TMAC is found to be lower than one, ranging from 0.75 to 0.85.

1. Introduction

The emergence of microelectromechanical systems (MEMS) as an important technology has raised a variety of new scientific questions related to the application of conventional tools of analysis to the unfamiliar world of micron-sized fluidic systems. Due to their small size, the surface area to volume ratio in MEMS can be large and thus surface effects, such as viscous interactions and surface chemistry, become relatively more important than is typically true in a larger-scale device. As an example of this scaling one can consider micromachined accelerometers, which are typically composed of a vibrating proof mass suspended a few microns from a stationary substrate. With such small clearances, viscous (squeeze-film) damping in the small gap is typically quite high, dominating the performance of the device. In order to minimize the damping, the gap is often vented using perforations in the proof mass, or packaged in vacuum. Despite these steps, viscous damping still limits device performance and is often poorly predicted using conventional continuum and crude non-continuum analysis (such as a pressure-dependent effective viscosity). One explanation for the lack of agreement between experiment and prediction is often that some kind of 'new physics' might be required to explain experimental observations for such micron-sized systems.

One source of such 'new physics' is the possibility that, at such small scales, non-continuum effects become important to the fluid–surface interactions, including the presence of slip flow and incomplete momentum and energy accommodation between

the gas and the substrate. The latter possibility is a reasonable suspicion given that the surface of MEMS is often a highly polished crystal face of the silicon substrate and such ordered surfaces are known to exhibit sub-unity accommodation (e.g. Seidl & Steinheil 1974). The purpose of this paper is to explore the basis for incomplete accommodation in MEMS devices.

1.1. *Models for slip flow*

Slip flow, which represents a rarefied gas phenomenon in which the common no-slip boundary condition breaks down at scales commensurate with the mean free path of the gas, is commonly described by the Maxwellian (Maxwell 1879) boundary condition for the fluid velocity, u, at a solid surface ($y = 0$):

$$u(y = 0) = \lambda \frac{2 - \sigma}{\sigma} \left. \frac{\partial u}{\partial y} \right|_{y=0}, \tag{1.1}$$

where λ is the mean free path of the gas. The constant σ is the tangential momentum accommodation coefficient (TMAC) which can vary from zero (specular accommodation) to one (complete, or diffuse accommodation). Although Maxwell's original formulation used a slightly different argument, the most intuitive description of the TMAC is that it represents the average streamwise (or tangential) momentum exchange between impinging gas molecules and the solid surface:

$$\sigma = \frac{u_r - u_i}{U_w - u_i}, \tag{1.2}$$

where u_i is the average incident streamwise velocity, u_r is the average reflected streamwise velocity and U_w is the streamwise velocity of the solid surface. For most gas–surface interactions at macroscopic (engineering) conditions, $\sigma = 1$, is the most appropriate choice.

Many researchers have measured the TMAC under a variety of conditions (for example Seidl & Steinheil 1974; Thomas & Lord 1974; Nakarjakov *et al.* 1995). For the most part, the test conditions have been at high vacuum, and have used molecular beams impinging on carefully prepared substrates. Very few, if any results are available at atmospheric conditions and using 'as-prepared' materials. Although the TMAC should not be affected by operating pressure or incidence angle, the surface conditions (level of absorbed materials and surface roughness, etc.) can affect the TMAC and for this reason, a study of MEMS surfaces at 'standard' conditions is of interest.

1.2. *Microchannel flows*

In recent years, the high-Knudsen-number regime has become accessible to experiments at atmospheric conditions by using microfabricated flow channels. Pfahler *et al.* (1991) and subsequently Harley *et al.* (1995) presented some of the first analytic and experimental work on rarefied microchannel flows and demonstrated the existence of slip flows in microchannels by observing an increase in the mass flow through the channel over what would be predicted using continuum (non-slip) calculations. However, the fabricated channels did not possess well-controlled surface structure (the channel was made by the bonding of dry-etched silicon and glass). In addition, they used a single-tank accumulation technique to measure the mass flow which is susceptible to thermal fluctuations and thus restricted their measurements to relatively large mass flows (this is discussed in more detail in § 3.1). Pong *et al.* (1994) presented results from experiments on microchannels, fabricated using surface micromachining

techniques with integrated pressure transducers, and reported pressure distributions measured along the length of the channel. Subsequent experiments by Shih *et al.* (1996) presented mass flow measurements and pressure distributions which were not in agreement with any theory. However, some questions remain about the dimensional tolerances of their microchannels (which are fabricated by surface micromachining techniques) and the accuracy of the mass flow measurement technique, which, like that of Harley *et al.* (1995), was a single-tank accumulation technique and is thus very sensitive to thermal fluctuations for these low mass flow regimes. Arkilic & Breuer (1993) and Arkilic, Schmidt & Breuer (1997*b*) explored, using a simple analysis, the effects of rarefaction and variable density in long microchannels, matching both the experimental data of Harley *et al.* (1995) and the measured pressure distributions of Pong *et al.* (1994).

Experimental results were also presented by Arkilic, Schmidt & Breuer (1994, 1997*b*). In this work, the flow rate of helium through carefully fabricated microchannels was measured and it was demonstrated that, as predicted, rarefaction was present in the microchannel flow. In addition, the theory of Arkilic *et al.* (1997*b*) was validated at these low flow rates. Although this series of experiments indicated excellent agreement with theory, the extraction of the TMAC requires an even more sensitive and more extensive series of measurements. It is this that forms the focus of the present paper.

Finally, it is worth noting that numerical approaches to rarefied flows in microchannels have also been explored using both slip-flow Navier–Stokes equations with higher-order boundary conditions (Beskok & Karniadakis 1999) as well as direct simulation Monte Carlo techniques (Piekos & Breuer 1995, 1996; Beskok & Karniadakis 1993, 1999 and most recently Cai *et al.* 1999). Such approaches have confirmed experimental and analytical results, although they still need the TMAC as an empirical input.

1.3. *Present work*

The present paper extends significantly the experimental work presented previously by our group (Arkilic *et al.* 1997*b*) in a number of ways. First and foremost, the sensitivity and accuracy of the pressure and mass flow measurements have been greatly enhanced using new hardware and improved experimental protocols. This additional precision allows not only verification that slip flow occurs at the micron-scale (not surprisingly), but has further allowed determination of the TMAC from those mass flow measurements. The determination of the TMAC is accomplished using a regression analysis, presented in § 2.1. Lastly, our previous work was conducted solely for helium flows, in which rarefaction is apparent in relatively large channels and at high pressures since the mean free path is so large. The present paper reports on experiments (and corresponding TMAC) for nitrogen, carbon dioxide and argon – all gases of larger molecular weight in which the accurate measurement of rarefaction is harder to achieve.

2. Background theory

A theoretical model for slip flow in long channels was reported by Arkilic *et al.* (1997*b*). The key assumptions and results are reported here for completeness and convenience. In this model, the gas is assumed to be isothermal and represented by the ideal gas equation of state. The compressible Navier–Stokes equations are solved

with a Maxwellian slip boundary condition which has the non-dimensional form

$$\tilde{u}|_w = \frac{2-\sigma}{\sigma} K \left.\frac{\mathrm{d}\tilde{u}}{\mathrm{d}\tilde{y}}\right|_w, \tag{2.1}$$

where $\tilde{u}$ and $\tilde{y}$ are the non-dimensionalized streamwise velocity and wall-normal coordinate (normalized by the mean exit velocity and channel height, H, respectively) and K is the Knudsen number, defined as the ratio of the mean free path, λ, to the channel height ($K = \lambda/H$). The subscript 'w' denotes evaluation at the wall, $y/H = \pm 1/2$. This boundary condition is strictly only valid for small Knudsen numbers ($K < 0.3$).

Upon expansion of the governing equations in the small parameter defined by the channel height-to-length ratio, Arkilic *et al.* (1997*b*) derived a system of equations, which upon solving at the lowest order describe a locally two-dimensional Poiseuille flow. However, due to the large pressure drop, the gas density changes along the length of the channel, resulting in a nonlinear pressure distribution, $\tilde{p}$, given by

$$\tilde{p}(\tilde{x}) = p(x/L)/P_o = -6\frac{2-\sigma}{\sigma}K_o + \sqrt{\left(6\frac{2-\sigma}{\sigma}K_o\right)^2 + \left(1 + 12\frac{2-\sigma}{\sigma}K_o\right)\tilde{x} + \left(\mathscr{P}^2 + 12\frac{2-\sigma}{\sigma}K_o\mathscr{P}\right)(1-\tilde{x})}, \tag{2.2}$$

where $\mathscr{P}$ is the inlet-to-outlet pressure ratio, P_i/P_o, and the subscripts i and o refer to inlet ($x = 0$; $\tilde{x} \equiv x/L = 0$) and outlet ($x = L$; $\tilde{x} \equiv x/L = 1$) conditions respectively. The mass flow is also found from the zeroth-order solution:

$$\dot{m} = \frac{H^3 W P_o^2}{24\mu L \mathscr{R} T}\left(\mathscr{P}^2 - 1 + 12\frac{2-\sigma}{\sigma}K_o(\mathscr{P}-1)\right), \tag{2.3}$$

where μ is the fluid viscosity, T the temperature and $\mathscr{R}$ the gas constant. L and W are the channel length and width respectively. Note that, for a given inlet and outlet pressure condition, the rarefaction acts to increase the observed mass flow and that as the pressure ratio decreases, the effect of slip makes a more significant contribution to the total mass flow. Also, as the outlet pressure increases for a given inlet pressure, or as the characteristic dimension increases, the rarefaction contribution diminishes.

With the exception of the TMAC, all variables in the expression for the mass flow (equation (2.3)) are known or are measurable and we can thus use this expression to determine the TMAC from mass flow–pressure characteristics of the microchannel.

2.1. *Determination of TMAC*

We can use and extend this analytic result to determine the TMAC for a given fluid–surface interaction. Making an analogy to Ohm's law where the differential pressure applied across the channel (ΔP) is analogous to the potential and the mass flow is analogous to the current, the flow conductance, $\mathscr{C}$, can be defined by

$$\mathscr{C} = \frac{\dot{m}}{\Delta P} = \frac{H^3 W}{12\mu L R T}\bar{P} + \frac{H^3 W}{2\mu L R T}\frac{2-\sigma}{\sigma}K_o P_o, \tag{2.4}$$

where $\Delta P = P_i - P_o$ is the differential pressure across the channel. The conductance can be written as

$$\mathscr{C} = \mathscr{A}\bar{P} + \mathscr{B}, \tag{2.5}$$

where

$$\mathscr{A} = \frac{H^3 W}{12\mu LRT}, \tag{2.6}$$

$$\mathscr{B} = \frac{H^3 W}{2\mu LRT}\frac{2-\sigma}{\sigma}K_o P_o \tag{2.7}$$

are constants, and $\bar{P} = (P_i + P_o)/2$ is the average of the inlet and outlet pressures (from here on referred to as the mean pressure).† Note that $\mathscr{A}$ is independent of the TMAC.

One could extrapolate this line to $\bar{P} = 0$ to determine the intercept, $\mathscr{B}$, and thus derive the TMAC. However, this is problematic, since it relies heavily on data in the free-molecular flow regime, where the theory becomes more and more tenuous. A preferable alternative is to normalize the measured mass flow by $(P_i^2 - P_o^2)$:

$$\frac{\dot{m}}{P_i^2 - P_o^2} = \frac{H^3 W}{24\mu LRT} + \frac{H^3 W}{4\mu LRT}\frac{2-\sigma}{\sigma}K_o P_o \frac{1}{\bar{P}}, \tag{2.8}$$

or

$$\frac{\dot{m}}{P_i^2 - P_o^2} = \frac{\mathscr{A}}{2} + \frac{\mathscr{B}}{2}\frac{1}{\bar{P}}, \tag{2.9}$$

where $\mathscr{A}$ and $\mathscr{B}$ are defined above. If the measured mass flow (weighted by the inverse of the difference between the squares of the inlet and outlet pressures, $\dot{m}/(P_i^2 - P_o^2)$) is plotted versus inverse mean pressure $2/(P_i + P_o)$, then the intercept of this line (which corresponds to the continuum limit) is independent of the TMAC while the slope of the line can be used to extract the TMAC. This weighting of the data provides a more attractive method of extracting the TMAC and is similar to the temperature jump (TJ) method which is used to derive experimental values for the energy accommodation coefficient (Goodman & Wachman 1876).

3. Experimental apparatus and procedure

The microchannels were fabricated in the MIT Microsystems Technology Laboratory using a fabrication process similar to our previous experiments (Arkilic *et al.* 1997*b*) and reviewed here for convenience. The fabrication sequence is shown schematically in figure 1, and a scanning electron micrograph of the resulting channel is shown in figure 2. To begin, a thick (1.33 μm) thermal oxide layer was grown on a double-polished silicon wafer. This defines the channel thickness. The thermal oxide was chosen as it forms a very uniform film over the wafer, thus ensuring good control of the channel thickness. The channel geometry, entrance and exit plena were then etched into the silicon oxide using buffered hydroflouric acid. A silicon nitride layer was deposited to protect the channel. The entrance and exit ports were then patterned and etched using a 20% potassium hydroxide solution. The channel was sealed by fusion bonding a second 'capping' wafer onto the top of the channel wafer. Bonding was achieved by contacting the wafers and then annealing at 1000 °C for 70 minutes. The bonded wafer was finally diced into smaller chips for handling, thus completing the fabrication sequence.

The fabrication sequence has a number of features that are worth highlighting.

† Note that, due to the nonlinear pressure distribution within the channel, $\bar{P}$ is not the same as the mean pressure within the channel.

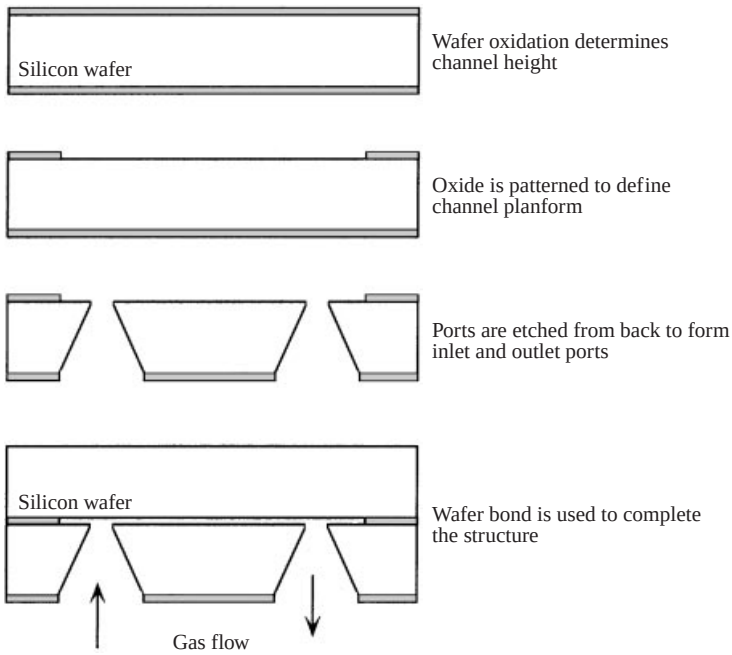

FIGURE 1. Schematic depiction of channel fabrication sequence. Adapted from Arkilic *et al.* (1997*b*).

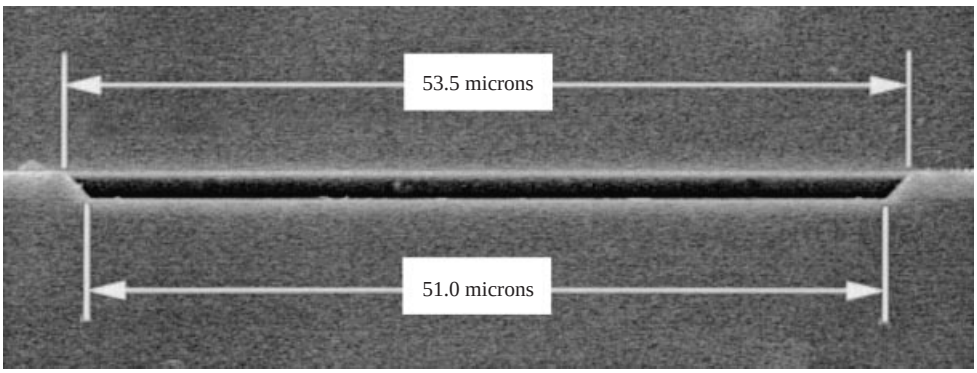

FIGURE 2. Scanning electron micrograph of microfabricated channel, shown end-on.

(*a*) The channels are long enough (7500 microns) such that entrance effects are negligible and can be safely ignored ($L/H > 5000$). In addition, the theory, which relies on a small channel height-to-length ratio is clearly valid.

(*b*) The channels are wide, with an aspect ratio (W/H) of approximately 40. Since three-dimensional effects are proportional to the inverse of the aspect ratio squared (White 1991), we can safely assume two-dimensional flow (also assumed in the analysis).

(*c*) The oxide layer that defines the channel height is very uniform over the channel length. This is a characteristic of thermal oxidation of silicon and one which can be easily confirmed during the channel fabrication process, prior to wafer bonding. This property is one of the reasons that this processing route was adopted for these experiments.

Parameter	Nominal value (μm)	Uncertainty μm)
Length (L)	7490	± 1
Width (w)	52.3	± 0.3
Height (H)	1.33	± 0.01
Maximum surface roughness	$\leqslant 0.65 \times 10^{-3}$	—

TABLE 1. Geometry of microfabricated channels. The measurements were made using Dektak and Wyco surface profilometers.

(*d*) The top and bottom surface of the channel are identical and are composed of polished silicon crystal with a thin layer of 'native' oxide (oxide that grows naturally on a silicon surface exposed to ambient air). This surface is very smooth, uniform and, as with the channel height, can be well characterized before the wafer-bonding step. This feature is in contrast to channels used by both Harley *et al.* (1995) and Pong *et al.* (1994). Harley *et al.* (1995) used a plasma-etched silicon channel with a glass capping layer. This resulted in a somewhat rough lower surface and dissimilar materials on the lower and upper surface. Pong *et al.* (1994) used a dissolved sacrificial layer of PSG to define their channel. Although they did not report surface roughness, it is likely to be higher than that of polished silicon. In their case, the lower surface was silicon while the upper surface was formed by a silicon nitride membrane.

(*e*) The surfaces that form the channel are very thick (approximately 500 microns) and will not bend under the large pressures that are required to drive the flow through the channel. This ensures that the channel geometry is invariant with flow pressure. Although this has similar structural integrity to the channels used by Harley *et al.* (1995), the microchannels used by Pong *et al.* (1994) used a thin (1.2 micron) silicon nitride membrane to define the upper surface. This has the drawback that it is susceptible to deformation and rupture under the high pressures required to drive a flow through the long channel.

Table 1 summarizes the channel geometry as measured prior to the bonding step.

3.1. *Mass flow measurement*

As mentioned earlier, a highly accurate mass flow measurement was required for these experiments. Earlier experiments, both by our group (Arkilic 1994) and others (e.g. Pong *et al.* 1994) have used accumulation techniques in which the gas flowing through the channel accumulates in a reservoir, resulting in either a change in pressure (constant-volume technique) or a change in volume (constant-pressure technique). The difficulty with these methods is that the small mass flows are very difficult to measure accurately using a single tank accumulation. In particular very small changes in temperature can overwhelm the mass flow measurement due to thermal expansion of the gas. The present results use a very sensitive dual-tank accumulation technique, described and analysed in detail by Arkilic, Schmidt & Breuer (1998). The system is schematically shown in figure 3. Gas flows through the test channel and into the accumulation tank. The mass flow through the system can be inferred from a measurement of the differential pressure between the accumulation tank and a reference (or 'system') tank. This arrangement is very insensitive to temperature fluctuations and allows highly sensitive measurements of mass flows, with a sensitivity demonstrated to be as low as $7 \times 10^{-15}\,\mathrm{kg\,s^{-1}}$.

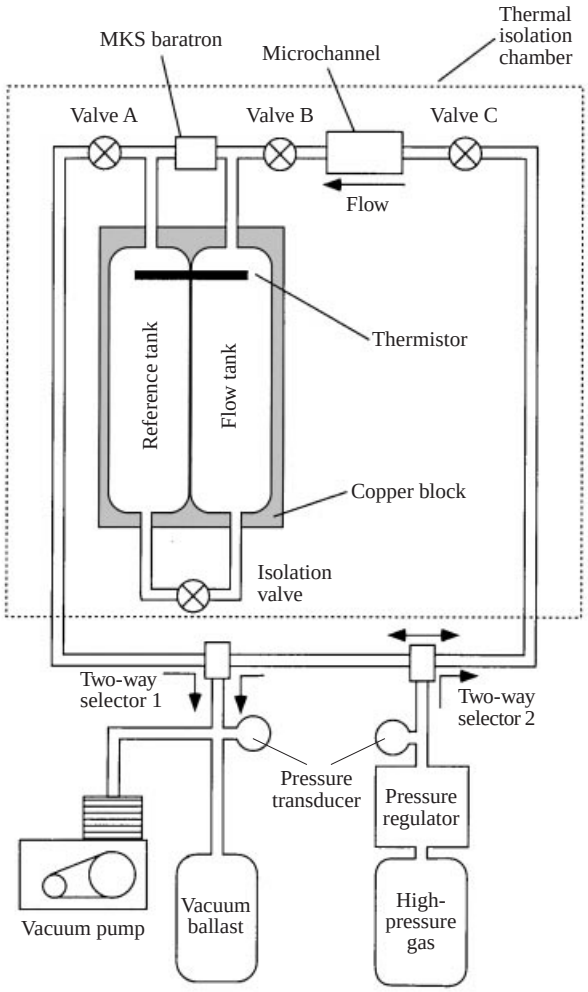

FIGURE 3. Schematic of mass flow measurement system. Adapted from Arkilic *et al.* (1998).

3.2. *Testing procedure*

The testing procedure was as follows. The reference tank and flow tank were first exposed to the desired outlet pressure by opening valves A, B, C and the isolation valve and setting the outlet pressure. Valve A was then closed and the system allowed to settle. The isolation valve was then closed. The valves, upon closing, inject mass into the piping due to the compression of the bellows. It was found that this unsteady mass injection led to thermal transients in the system. These were eliminated by closing the isolation valve very slowly, over 30 minutes (this was accomplished using a voltage-controlled pressure regulator to drive the pneumatically controlled isolation valve). After the isolation valve was closed, the system was again allowed to settle.

The flow test sequence consisted of three 10-minute intervals during which the differential pressure between the flow and reference tanks was measured. In the pre-flow measurement interval (interval I), the differential pressure was recorded for 10 min before the microchannel was pressurized. The flow was then initiated through the resistance by increasing the inlet pressure of the microchannel to the desired

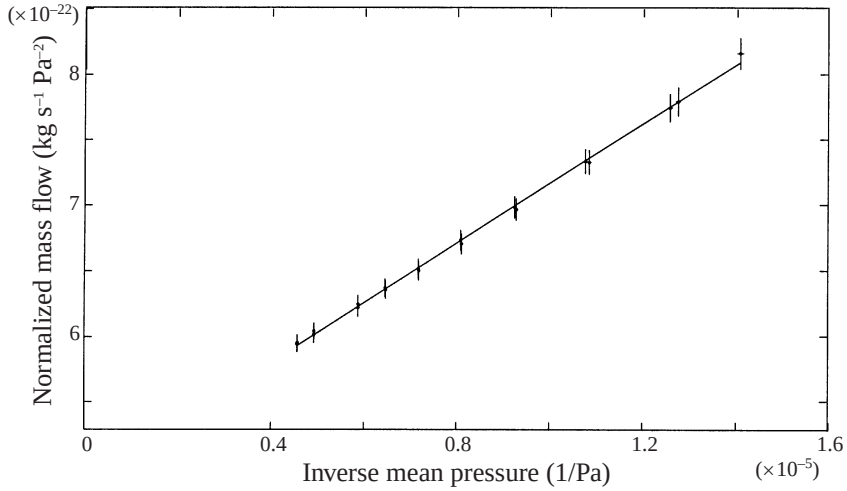

FIGURE 4. Data and least-squares fit (which is used to derive a value for the TMAC) for a representative set of argon flow experiments exhausting to an outlet pressure of 13 kPa. Two data points at each pressure represent measurements acquired on ramping the inlet pressure up and then down.

value by means of the voltage-controlled pressure regulator. It was found that by slowly ramping up the pressure over 10 s we were able to maintain quasi-steady (isothermal) conditions. Once at the desired inlet pressure, Δp was recorded for an additional 10 min (interval II). Finally, the inlet pressure was ramped back down over a time period of 10 s and Δp was recorded for another 10 min (the post-flow interval or interval III). Any ambient thermal variations during these three intervals was easily recognizable from measurements taken during the pre- and post-flow sequences (intervals I and III). These effects, if present, were removed using a multi-segment least-squares algorithm (Arkilic *et al.* 1998).

4. Results and discussion

The test conditions for the flow experiments are shown in table 2. At this range of working conditions, both the Reynolds and Mach numbers are approximately 10^{-2}, clearly in the region of validity for the isothermal, variable-density theory of Arkilic *et al.* (1997*b*). For each working gas and at each outlet Knudsen number, a suite of mass flow versus inlet pressure measurements were taken. The data were then normalized as described earlier and plotted as the normalized mass flow, $\dot{m}/(P_i^2 - P_o^2)$, versus the inverse mean pressure, $2/(P_i + P_o)$. A representative example of the experimental data normalized in this manner is shown in figure 4. The uncertainty bars shown in the figure are calculated using the definition of the normalized mass flow and the uncertainty in the mass flow, inlet and outlet pressures previously defined. As predicted by the theory (equation (2.8)) the data are well-described by a straight line fit. For the case shown in figure 4, the coefficient of determination for the linear least-squares fit is better than 0.99 and for all of the results presented in this paper the coefficient of determination was greater than 0.96. Note that the time taken to acquire each of these data sets (approximately 20 data points at a given outlet pressure) is roughly 12 hours due to the long times needed to ensure system stability and experimental accuracy.

Gas	Channel	P_i (kPa)	P_o (kPa)	K_o
Ar	1A, 2A	130–430	13–102	0.05–0.41
N_2	1B	132–430	16–101	0.05–0.34
CO_2	1B	135–430	15–100	0.03–0.44

TABLE 2. Range of test conditions.

4.1. *Experimentally determined viscosity*

As discussed earlier, the intercept of the normalized mass flow data as shown in figure 4, is determined solely by geometry and known gas quantities. This was used as a check of the quality of the experimental data. Using the theoretically derived definition of the intercept, $\mathscr{A}$ (2.6), we can derive an empirically determined coefficient of viscosity, μ_e:

$$\mu_e = \frac{H^3 W}{12 \mathscr{A} LRT}, \tag{4.1}$$

which can then be compared with the tabulated viscosity for the experimental flow conditions.

The empirical viscosities are shown as a function of outlet Knudsen number in figures 5(*a*), 5(*b*) and 5(*c*) for experiments conducted in argon, nitrogen and carbon dioxide respectively. Two sets of data are presented for argon. These represent measurements taken in two different channels. Each data point is plotted with its corresponding uncertainty. The dotted line indicates the tabulated value of μ for the working gas.

For the majority of the experiments the empirical viscosity is equal to the accepted value for the viscosity to within the uncertainty of the measurements, indicating that the experimental data are of high quality. The exception to this are three points at the low outlet Knudsen numbers for the carbon dioxide series, shown in figure 5(*c*). It is believed that the most likely reason for this anomalous result is a gas impurity introduced during the exchange of high-pressure gas tanks. (During flow experiments a substantial amount of high-pressure gas is 'consumed' by the pressure regulators, i.e. bled to the atmosphere.) However, since records of tank changes were not kept, this belief cannot be verified and the results cannot be outright rejected. However, measurements of TMAC based on these three data points should be regarded with caution. The flow measurements at this condition ($K = 0.032$) were repeated five times in a second series of experiments designed to check this anomalous result and to provide some data on repeatability. The experimentally determined viscosity for these points are also shown in figure 5(*c*). This series shows excellent repeatability and lies within the range of experimental uncertainty. These results increase our confidence in the data and reinforce the belief that the anomalous data present in figure 5(*c*) was, as suspected, due to accidentally introduced gas impurities. It also emphasizes the utility of the empirical viscosity (or any other means for comparing the measured value of $\mathscr{A}$ to its predicted value) as a valuable warning on the integrity of the data in these difficult experiments.

Although the theory developed earlier is strictly valid only at small values of K, the obtained values of μ_e suggest that it might remain valid at much higher values of K. This is, perhaps, not surprising. Asymptotic expansions are commonly found to be accurate well beyond their strict range of validity. In this case, however, one

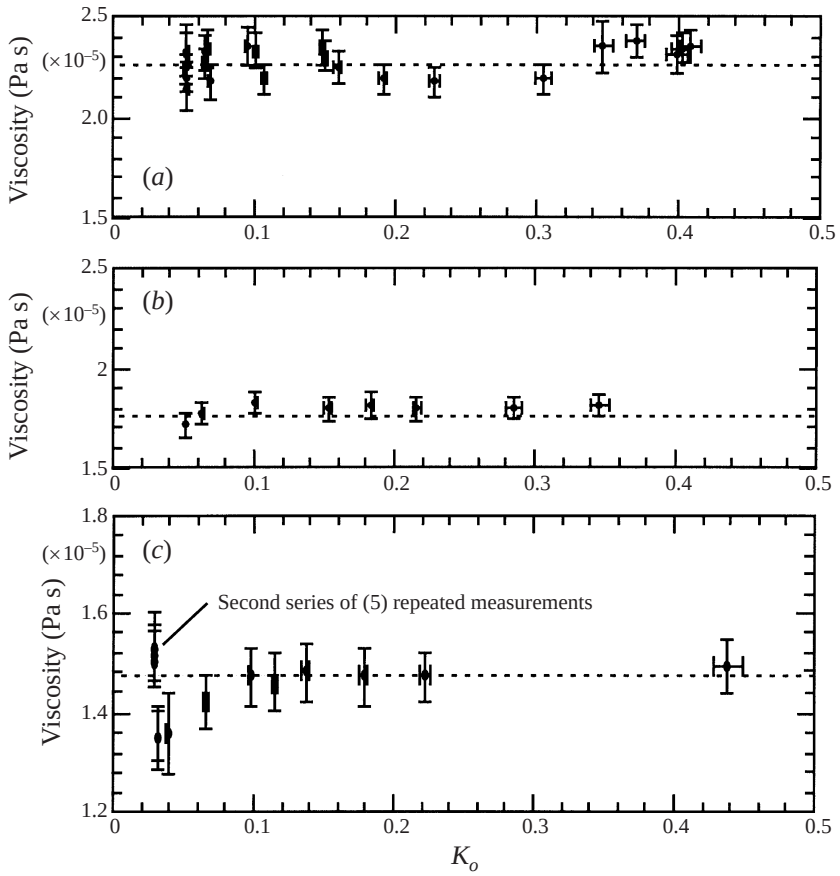

FIGURE 5. Empirical viscosity vs. outlet Knudsen number (*a*) Working gas: argon (data from two different channels). (*b*) Working gas: nitrogen. (*c*) Working gas: carbon dioxide. A second series of data was taken at one Knudsen number ($K = 0.032$) to assess repeatability.

possible reason for this extended validity might be due to the fact that the Knudsen number along most of the channel remains quite low (due to the high pressure along the length of the channel) and thus, even at relatively high exit Knudsen number conditions, most of the fluid in the channel sees conditions that are well within the strict definition of slip flow. In addition, the channel geometry is so simple that many of the correction terms that should come in at higher order (for example, from the Burnett equations) are not present due to the geometric simplicity of the long channel geometry. Thus, although we should place a limit of $K < 0.1$, the model might well hold for values of the Knudsen number far higher.

5. Normalized flow and TMAC measurements

Having established confidence in the accuracy of the data, we now proceed to determine the TMAC, σ, from the slope of the normalized mass flow. The results of this are shown in figures 6(*a*), 6(*b*) and 6(*c*) for argon, nitrogen and carbon dioxide respectively. As with the empirical viscosity measurements, two sets of argon data are reported, representing two different flow channels. Each of the data points in each figure corresponds to a separate set of flow experiments similar to those shown

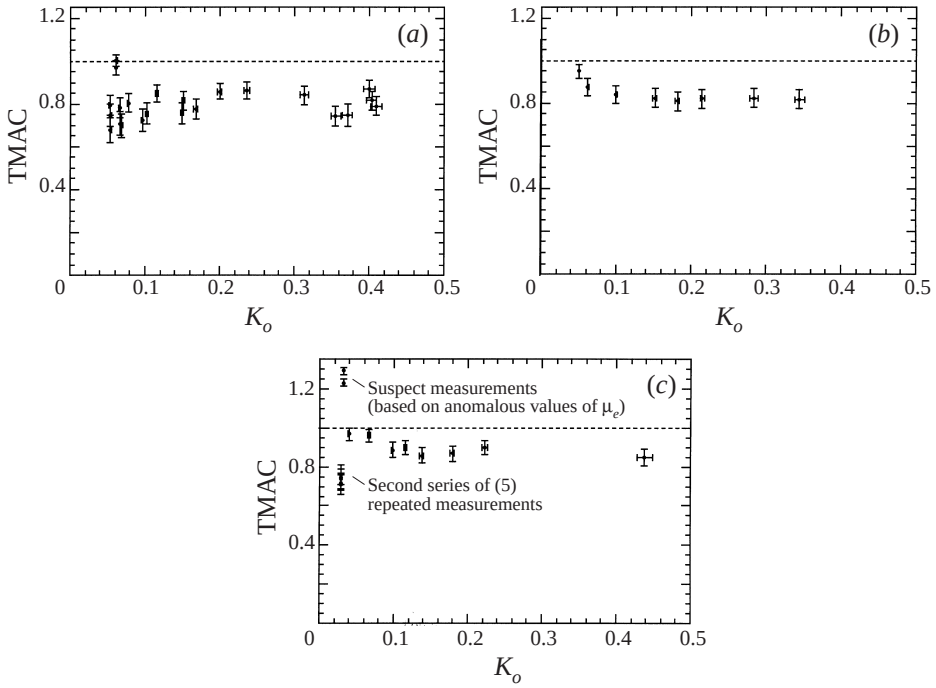

FIGURE 6. TMAC values as a function of outlet Knudsen number. (*a*) Argon: data from two distinct microchannels are presented (Series I and II). (*b*) Nitrogen. (*c*) Carbon dioxide: second a series of five measurements was made at $K_o = 0.032$ after observing the anomalous values of μ_e in order to check data consistency and repeatability.

in figure 4 and the figures are derived from the same data used to extract the experimentally determined viscosity, shown in figure 5.

There are two striking features of these results. First, for the majority of the tests, there is a significant deviation from unity of the TMAC value, with most of the values ranging between 0.75 and 0.85. Secondly, the value of the TMAC derived from the data is more or less constant with outlet Knudsen number. For the carbon dioxide data at low Knudsen number, the values of the TMAC shown are greater than one. However, these data should be discounted based on the anomalous values of μ_e corresponding to these conditions. The TMAC based on the second series of carbon-dioxide experiments (five experiments at the same outlet condition of $K = 0.032$) indicate sub-unity values of TMAC and are consistent with, though lower than, the values of TMAC derived from the first series of experiments.

Another interesting observation from figure 6(*b*) is an apparent increase in the TMAC as the outlet Knudsen number approaches zero. At this stage, we are unable to determine whether there is any physical reason for this change (such as channel 'aging') or whether this is simply a statistical quirk or an artifact of the experimental procedure. It is worth noting that (in all cases) the data were collected starting at high Knudsen number, and progressing to lower values of K. In addition, for this case, the channel was 'pristine' at the start of the experimental series. This might suggest that the TMAC increases slightly as the channel ages. However, at this stage the relevance of this observation is still not clear and will hopefully be addressed in future experiments.

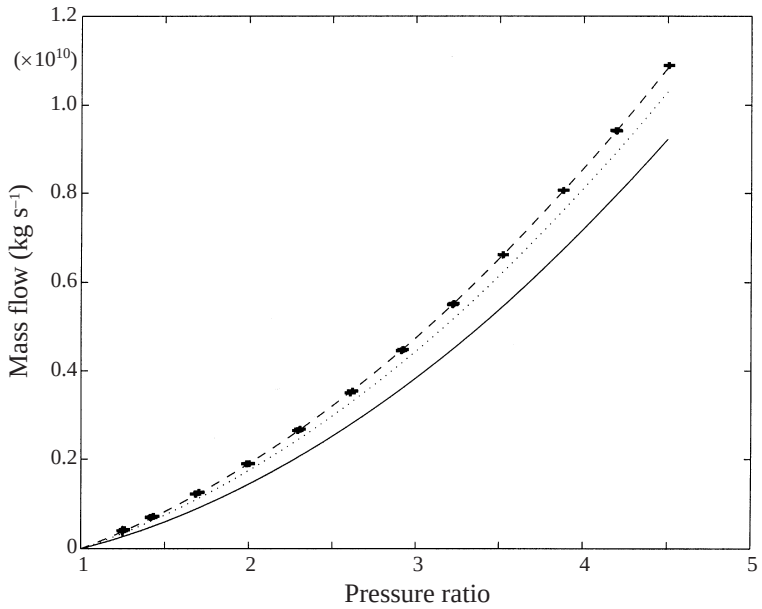

FIGURE 7. Mass flow versus pressure for argon with outlet Knudsen number of 0.053: ——, the continuum solution ($K = 0$); · · · · · ·, the analytic solution for rarefied flow with complete accommodation ($K = 0.053$, $\sigma = 1$); - - - - -, the analytic solution for rarefied flow, incomplete accommodation, using the value of TMAC derived from the experimental data ($k = 0.053$, $\sigma = 0.8$); x, experimental measurements and their size represents the uncertainty in the experimental measurements using the current configuration.

As a final step, it is useful to take the value of the TMAC derived using the above procedures and to plot the dimensional mass flow against the applied pressure, compared with the corresponding theoretical prediction. This is shown in figure 7 for the case of argon, flowing at $K_o = 0.053$ and using $\sigma = 0.8$. The close agreement is evident, confirming both the accuracy of the experiments and the good applicability of the low Knudsen number theory to this flow regime. The relevance of the sub-unity accommodation can be seen by comparing the dotted and dashed lines which correspond to complete and incomplete accommodation respectively.

6. Concluding remarks

The results presented here clearly show a sub-unity accommodation coefficient for prime silicon substrates. The TMAC is (as expected) independent of pressure, reinforcing the credibility of these results. What is particularly intriguing about these results is that they are achieved at relatively standard operating conditions for MEMS and that the surfaces and gases used are not by any means unusual (in comparison, for example, with some of the previous TMAC measurements in which the surfaces were painstakingly prepared and isolated from contamination). Thus, one would expect that these phenomena are observed in standard MEMS devices and that such sub-unity accommodation should be accounted for in modelling of viscous interactions.

A word should be added on the difficulty of such measurements. The mass flows in MEMS are so small and so sensitive to small variations in geometry, temperature, etc. that very careful measurements are required to differentiate between slip, TMAC

and other extraneous effects. In the present work, this necessitated very carefully controlled device fabrication, and the development of a mass flow measurement system that was previously not available. With this system now in place, we anticipate extending such studies to include different gas–surface combinations and the effects of surface roughness and adsorbants such as moisture or chemical contaminants.

We are most grateful for the financial support of NSF, DARPA, AFOSR and Physical Science Incorporated who, at various times and at various levels, make the work possible. We should also like to acknowledge Harold Wachman and Isaac Greber who both contributed valuable suggestions and insight. Some of the data reported in this paper was presented at the Rarefied Gas Dynamics Symposium, Beijing, China (Arkilic, Schmidt & Breuer 1997*a*).

REFERENCES

Arkilic, E. 1994 Gaseous flow in micron-sized channels. Master's thesis, Massachusetts Institute of Technology, Cambridge, MA.

Arkilic, E., Schmidt, M. & Breuer, K. 1994 Gaseous flow in microchannels. In *Application of Microfabrication to Fluid Mechanics, ASME Winter Annual meeting, Chicago, IL* (ed. P. R. Bandyopadhyay), pp. 57–65.

Arkilic, E., Schmidt, M. & Breuer, K. 1997*a* TMAC measurement in silicon micromachined channels. In *Proc. 20th Symp. on Rarefied Gas Dynamics, Bejiing, China* (ed. C. Shen). Peking University Press.

Arkilic, E., Schmidt, M. & Breuer, K. 1998 Sub-nanomol flow measurement near atmospheric pressure. *Exps. Fluids* **25**, 37–41.

Arkilic, E. B. & Breuer, K. S. 1993 Gaseous flow in microchannels. *AIAA Paper* 93–3270.

Arkilic, E. B., Schmidt, M. A. & Breuer, K. S. 1997*b* Gaseous slip flow in long microchannels. *J. Microelectromech. Systems* **6**, 167–178.

Beskok, A. & Karniadakis, G. 1993 Simulation of heat and momentum transfer in micro-geometries. *AIAA Paper* 93–3269.

Beskok, A. & Karniadakis, G. 1999 A model for flows in channels, pipes and ducts at micro- and nano-scales. *J. Microscale Thermophys. Engng* **3**, 43–77.

Cai, C.-P., Fan, J., Boyd, I. & Candler, G. 1999 Direct simulation methods for particle simulation of micro-channel flows. *AIAA Paper* 99–3801.

Goodman, F. & Wachman, H. 1976 *Dynamics of Gas-Surface Scattering*. Academic.

Harley, J., Huang, Y., Bau, H. & Zemel, J. 1995 Gas flow in micro-channels. *J. Fluid Mech.* **284**, 257–274.

Maxwell, J. C. 1879 On stress in rarefied gases arising from inequalities of temperature. *Phil. Trans. R. Soc. Lond.* Reprinted in *The Scientific Papers of James Clerk Maxwell*. Dover.

Nakarjakov, A., Borisov, S., Sharipov, F. & Suetin, P. 1995 The effect of the surface chemical composition on a free molecular gas flow in a cylindrical channel. In *Rarefied Gas Dynamics* (ed. J. Harvey & G. Lord). Oxford University Press.

Pfahler, J., Harley, J., Bau, H. & Zemel, J. 1991 Gas and liquid flow in small channels. In *Micromechanical Sensors, Actuators, and Systems, ASME Winter Annual meeting, Atlanta, GA*, pp. 49–59.

Piekos, E. & Breuer, K. S. 1995 Computational modelling of micromachined devices. *AIAA Paper* 95–2089.

Piekos, E. & Breuer, K. S. 1996 DSMC modeling of micromechanical devices. *Trans. ASME: J. Fluids Engng* **118**, 464–469.

Pong, K., Ho, C.-M., Liu, J. & Tai, Y.-C. 1994 Non-linear pressure distribution in uniform microchannels. In *Application of Microfabrication to Fluid Mechanics, ASME Winter Annual meeting, Chicago, IL*, pp. 51–56.

Seidl, M. & Steinheil, E. 1974 Measurement of momentum accommodation coefficients on surfaces characterized by Auger spectroscopy, Sims and LEED. In *Rarefied Gas Dynamics* (ed. M. Becker & M. Fieberg). DFVLR Press.

Shih, J., Ho, C., Liu, J. & Tai, Y. 1996 Monatomic and polyatomic gas flow through uniform microchannels. In *Application of Microfabrication to Fluid Mechanics, ASME Winter Annual meeting, Atlanta, GA*, pp. 197–203.

Thomas, L. & Lord, R. 1974 Comparative measurements of tangential momentum and thermal accommodations on polished and on roughened steel spheres. In *Rarefied Gas Dynamics* (ed. K. Karamcheti). Academic.

White, F. M. 1991 *Viscous Fluid Flow*. McGraw-Hill.